

# Organic carbon content and carbon isotope variations across the Permo-Triassic boundary in the Gartnerkofel-1 borehole, Carnic Alps, Austria

M. E. Brookfield<sup>1</sup>  · W. S. Wolbach<sup>2</sup> · A. G. Stebbins<sup>1</sup> · I. Gilmour<sup>3</sup> · D. R. Roegge<sup>4</sup>

Received: 3 February 2017 / Revised: 6 May 2017 / Accepted: 22 August 2017 / Published online: 12 December 2017  
© Science Press, Institute of Geochemistry, CAS and Springer-Verlag GmbH Germany, part of Springer Nature 2017

**Abstract** The Gartnerkofel borehole is one of the most thoroughly studied and described Permo-Triassic sections in the world. Detailed bulk organic carbon isotope studies show a negative base shift from  $-24\text{‰}$  to  $-28\text{‰}$  in the Latest Permian which latter value persists into the Earliest Triassic after which it decreases slightly to  $-26\text{‰}$ . Two strongly negative peaks of  $> -38\text{‰}$  in the Latest Permian and a lesser peak of  $-31\text{‰}$  in the Early Triassic are too negative to be due to a greater proportion of more negative organic matter and must be due to very negative methane effects. The overall change to more negative values across the Bulla/Tesero boundary fits the relative rise in sea level for this transition based on the facies changes. A positive shift in organic carbon isotope values at the Late Permian Event Horizon may be due to an increase in land-derived organic detritus at this level—a feature shown by all

Tethyan Permo-Triassic boundary sections though these other sections do not have the same values. Carbonate carbon isotope trends are similar in all sections dropping by 2–3 units across the Permo-Triassic boundary. Gartnerkofel carbonate oxygen values are surprisingly, considering the ubiquitous dolomitization, compatible with values elsewhere and indicate reasonable tropical temperatures of  $60\text{ °C}$  in the Latest Permian sabkhas to  $20\text{--}40\text{ °C}$  in the overlying marine transition beds. Increased land-derived input at the Late Permian Event Horizon may be due to offshore transport by tsunamis whose deposits have been recognized in India at this level.

**Keywords** Organic · Carbon · Isotopes · Permo-Triassic · Gartnerkofel · Austria

✉ M. E. Brookfield  
mbrookfi@hotmail.com

W. S. Wolbach  
wendywolbach@gmail.com

I. Gilmour  
ia.in.gilmour@open.ac.uk

D. R. Roegge  
droegge@embarqmail.com

<sup>1</sup> School for the Environment, University of Massachusetts at Boston, Boston, MA 02125, USA

<sup>2</sup> Department of Chemistry, DePaul University, Chicago, IL 60614-2245, USA

<sup>3</sup> Department of Physical Sciences, Planetary and Space Sciences, The Open University, P.O. Box 197, Milton Keynes MK7 6BJ, UK

<sup>4</sup> Department of Chemistry, Illinois Wesleyan University, Bloomington, IL 61701-1792, USA

## 1 Introduction

The Gartnerkofel borehole is one of the most thoroughly studied and described Permo-Triassic sections in the world (summary in Holser et al. 1989, 1991). Although Klein (1991) included organic carbon contents in his more inclusive study of elements, the results of detailed organic carbon isotope studies across the PTr boundary in the core have only been reported in a brief abstract (Wolbach et al. 1994). In view of the importance of such studies in other Permo-Triassic sections, this paper summarizes these analyses of the total Gartnerkofel organic carbon, organic carbon isotopes, together with carbonate carbon and oxygen isotopes from Magaritz and Holser (1991), compares them with the total organic carbon analyses of Klein (1991) on the same samples, and compares our Gartnerkofel carbon patterns to other Permo-Triassic Tethyan sections.

## 2 Geology

The Gartnerkofel core was drilled in 1986 near the western end of the Permian Tethys Sea in a shallow-water shelf area interpreted as a currently eastward facing carbonate ramp (Brandner et al. 2009) (Figs. 1, 2).

Over most of its outcrop, the Late Permian Bellerophon Formation consists of thick carbonate-sulphate succession deposited in marginal (sabkha) to shallow shelf marine conditions with the top  $\sim 1$  m (Bulla member) consisting of more normal marine highly fossiliferous dark bioclastic wackestone, packstone and interbedded thin marls limestone with calcareous algae, foraminifera, mollusks and brachiopods (Noé 1987; Farabegoli et al. 2007). A top erosional surface on the Bulla Member is sharply overlain by the Tesero member of the Werfen Formation, which consists of diverse micrite, microbialites and marls interbedded with oolitic, peloidal and bioclastic packstones (Farabegoli et al. 2007). The Tesero member blankets the underlying diverse Bulla Member facies, and varies little and irregularly (between 3 and 5 m) across the entire area, though it is absent between Bulla and Gartnerkofel (Noé 1987).

The previously proposed carbonate ramp interpretation of the Tesero oolite section (Brandner et al. 2009) is incompatible with the limited thickness and facies variations shown in the sections, and with the juxtaposition of very different sections across Alpine thrusts, with large translations of tens of km, within the Dolomites (Doglioni 1987). Thus the Tesero oolite is missing in the San Antonio

section though present in the thrust sheets on either side (Fig. 2). Furthermore the ramp interpretation (as shown in Fig. 2b) is arbitrarily based on arranging Tesero oolite sections and the burrowed datum on which they rest, in a line downstepping to the east: the thinning of the lowermost oolite from Tramin to Gartnerkofel (interrupted by the fault-enclosed San Antonio section) is typical of carbonate platforms like the Bahama Bank, where marginal oolite shoals thin and pass into pelletoidal finer sediments towards the interior of the platform (Harris et al. 2015). A flat carbonate platform environment fits the lack of horizontal but marked vertical facies change (during sea level variations) far better, and was the interpretation shown by Noé (1987) in the first comprehensive study of the PTr boundary sections in the area (Fig. 2c).

Furthermore, the Permian paleomagnetism of the Dolomites shows around  $50^\circ$  anticlockwise rotations of the southern Alps relative to central Europe during large post-Permian lateral movements and disruption of the Adria block (Muttoni et al. 2013) and can thus not be compared to units now adjacent to it, like the Lombardy Verrucano to the west across the Judicaria fault (Gaetani 2010).

The biodiversity drops markedly at the Bulla/Tesero contact but Permian brachiopods and bivalves persist into the Tesero Member (Posenato 2009). The first appearance datum (FAD) of the conodont *Hindeodus parvus* which defines the base of the Triassic is at 6 m above the base of the Tesero Member at Gartnerkofel, but only 2 m above the base at Bulla (Schönlaub 1991) (Fig. 2).

The main lithological change (the Late Permian Event Horizon, LPEH) from the Bulla to the Tesero Members thus does not co-incide with the main extinction, nor with the base of the Triassic as defined by *H. parvus*. The strata between the LPEH and the base of the Triassic are thus of great interest for interpreting environmental changes associated with the extinction.

## 3 Materials and methods

One set of PTr samples were used for all Gartnerkofel geochemical analyses (Klein 1991).

### 3.1 Wolbach and Gilmour methods

To cover the PTr boundary adequately, bulk C residues were isolated from samples between 115.95 and 330 m depth in the core, using HCl and HF–HCl procedures of Wolbach and Anders (1989). Organic carbon was separated from any elemental carbon using extended acid dichromate oxidation (Wolbach and Anders 1989). Residues were combusted to  $\text{CO}_2$  for mass-spectrometric analysis, yielding isotopic data, and weights for organic carbon. Carbon

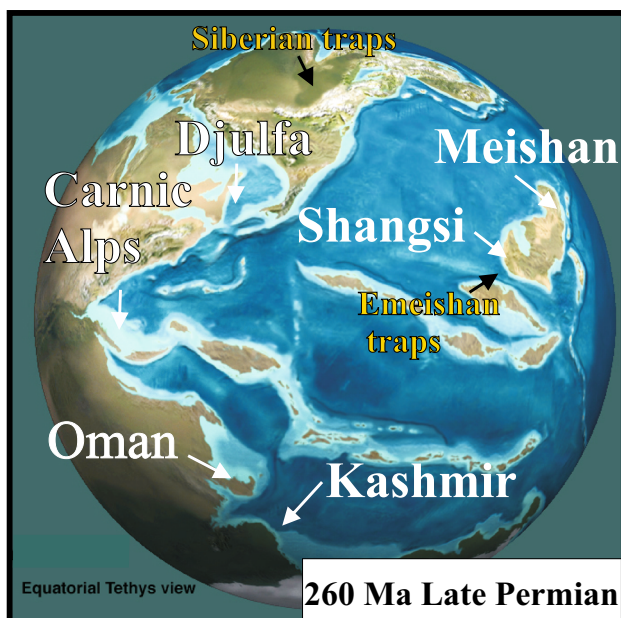


**Fig. 1** Late Permian palaeogeography (courtesy Ron Blakey) with places cited

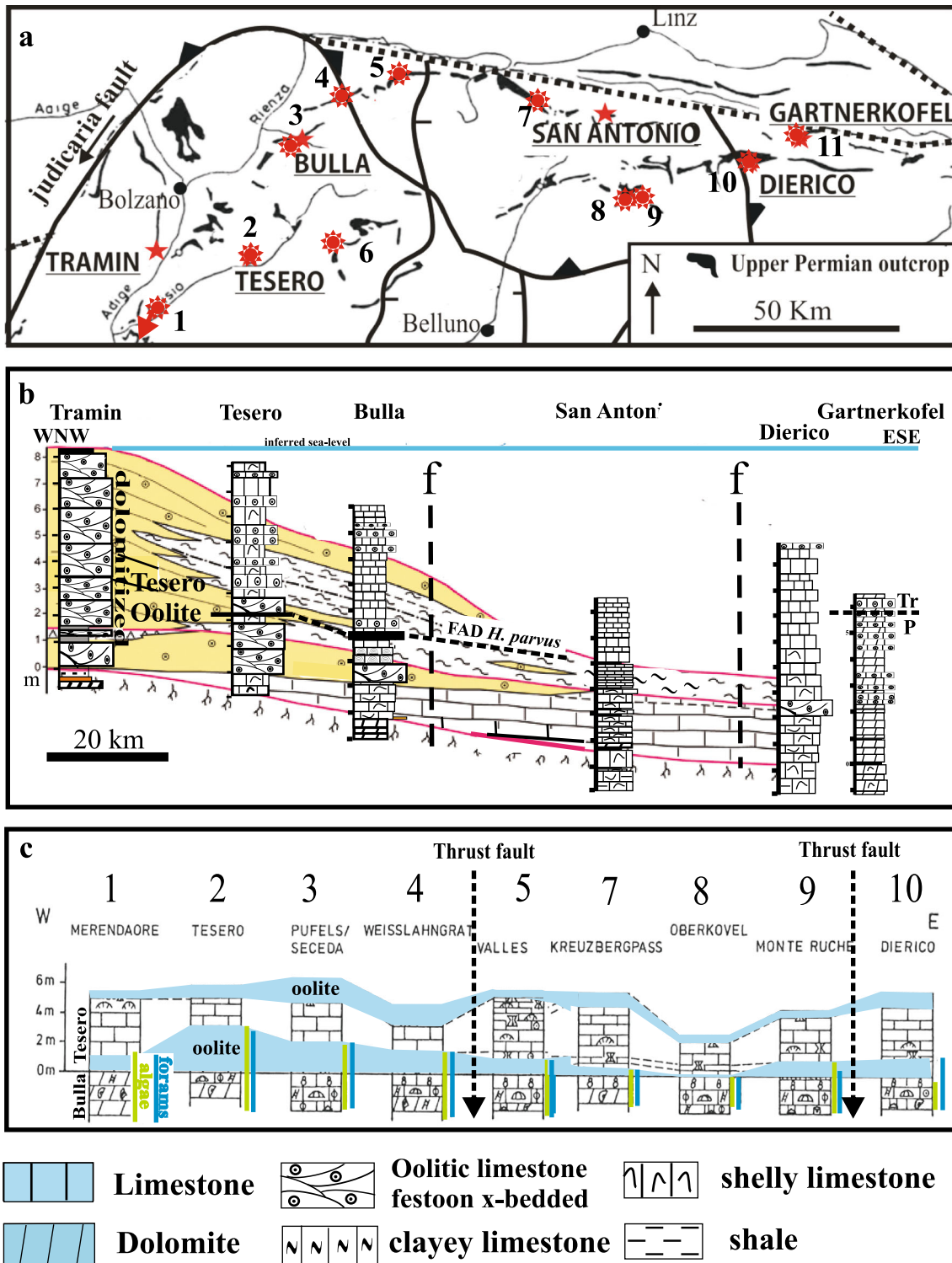


**Fig. 2** **a** Location of Gartnerkofel and other PTTr sections in the Dolomites, southern Alps. **b** Reconstructed cross-section of the Early Triassic carbonate ramp at the end of Tesero oolite deposition (after Brandner et al. 2009, Fig. 8), with representative sections. Note that the only Tramin, Tesero and Bulla sections are in the same tectonic unit, the other sections are across thrust faults, and actual thickness variation is nowhere greater than 5 m across a horizontal distance of over 130 km. **c** Thickness variation and persistence of Bulla and Tesero Oolite facies from west to east (from Noé 1987). *Source:* Stratigraphic columns: Tramin: Brandner et al. (2012); Tesero: Posenato (2009); Bulla: Farabegoli and Tonidandel (2012), Posenato (2009); San Antonio: Brandner (1988); Kraus et al. (2013); Dierico: Buggisch and Noé (1986); Gartnerkofel: Holser et al. (1991)

isotopes were measured on a VG SWIRA 24 mass spectrometer using sealed-tube combustion.

### 3.2 Klein (1991) methods

The carbon content was analyzed on separate aliquots of the powdered samples. For determination of total carbon ( $C_{\text{tot}}$ ) a 100 mg portion was weighed into a ceramic crucible by electronic balance. With a glass spoon about 2 g of LECOCEL (a Sn-W alloy) and 1 g of steel (7 ppm C, 14 ppm S) were added. The mixture was combusted in a furnace at 1400 °C, using oxygen (> 99.5% pure) as carrier gas. The evolved gas  $\text{CO}_2$  was measured in infrared cells by integrating its peaks. The system was calibrated with LECO calibration samples and with internal laboratory standard Bellerophon Dolomite A/1.

Each sample was analyzed two to four times. The relative standard deviations were < 1% for C. For determination of organic carbon ( $C_{\text{org}}$ ), 500 mg of powder were weighed into a porous filter crucible, leached three times with 8 mL 2 M HCl, rinsed ten times with deionized water, and filtered with a filtering flask. The crucibles were dried in an oven at 150° overnight. Measurements were carried out as for total C. Acid-soluble carbon ( $C_{\text{carb}}$ ) was calculated by difference.

## 4 Results

Total organic carbon and organic carbon isotopes of our study, together with the total organic carbon of Klein (1991), and carbonate carbon and oxygen isotope results of Magaritz and Holser (1991), plus the S and  $\delta^{34}\text{S}$  results of Pak and Holser (1991) are shown on Table 1 and Fig. 3.

In our study, the brown color of all carbonaceous residues and rapid disappearance of residue aliquots on dichromate oxidation, together with their carbon content (~ 100%); indicate that the residues were composed entirely of organic carbon. The organic carbon content of the sediments was relatively low (< 2000 ppm) except at 216 m (> 5000 ppm), and at 215 and 268 m (> 2000 ppm) (Table 1, Fig. 3). These high values correspond with lower negative  $\delta^{13}\text{C}_{\text{org}}$  values, which are in keeping with their inferred oceanic origin, as these samples were easily oxidized by dichromate—residual land-derived organic matter is much more difficult to destroy (Wolbach et al. 1994).

The total organic carbon results of Klein (1991) are divergent from ours and tend to be an order of magnitude higher (Table 1). The reasons for this are not entirely clear (we could not contact Peter Klein for comment), but could be due to: (a) sampling differences—unlikely, as we analyzed the same layers; (b) mineral acid differences—2 M HCl for Klein, 9 M HCl followed by 15 M HF/1 M HCl

for Wolbach, more aliphatic organic carbon would be destroyed by these methods—which would explain the lower Wolbach values; (c) destruction of silicates—by dissolving silicates, Wolbach freed up any carbon bound by the silicate crystal structure itself that carbon fraction would have been measured by Wolbach, but not by Klein—again this does not explain the lower Wolbach values; (d) oxidation—Wolbach made a concerted effort to destroy organics, then determine their isotopic values by difference whereas Klein measured organics directly, which might have missed silicate-encapsulated organics, but included any elemental carbon present with his  $C_{\text{org}}$  data and assumed it to be organic.

Nevertheless, the trends are the same in both analyses and the total organic values are all low in any case (Table 1, Fig. 3).

Our organic carbon isotope studies show a negative base shift of – 24‰ to – 28‰ in the upper Bellerophon Formation to – 26‰ to – 28‰ in the Tesero Member, which latter values persists into the earliest Triassic Mazzin Member, after which it decreases slightly to – 26‰ (Table 1, Fig. 3). Superimposed on this are two sharp negative peaks of > – 38‰ in the Latest Permian (at 286.33 and 252 m depth) and a broader negative peak of > – 31‰ (215.07–207.14 m depth) in the Early Triassic (Fig. 3). The two negative peaks in the upper Bellerophon Formation are not recorded in Wolbach et al. (1994) as they did not plot the values below 242 m.

The  $\delta^{13}\text{C}_{\text{carb}}$  values show a gradual drop from the Bellerophon through the Tesero Member into the lower Mazzin Member, followed by subdued fluctuations (Fig. 3). This is consistent with the general average worldwide drop of – 2‰ across the PTr boundary (Korte et al. 2001).

The  $\delta^{18}\text{O}_{\text{carb}}$  values also show a gradual drop from the Bellerophon into the Tesero Member after which they remain fairly constant until some zigzags in the lower Mazzin Member at the same level as the organic carbon zigzag (Fig. 3). Although these beds show both Early and Late dolomitization (Boeckelmann and Magaritz 1991), and the oxygen isotopes therefore unlikely to be primary, and though the Gartnerkofel values are whole rock values, the significant fluctuations suggest that the oxygen isotopes in the section have not been homogenized. Under meteoric diagenesis Phanerozoic carbonate rocks show elevated Mn and decreasing Sr contents due to dissolution of primary carbonate and precipitation of carbonate cements (Brand and Veizer 1980): carbonate samples with Mn/Sr ratio of < 10 might still retain their primary isotopic signatures (Kaufman and Knoll 1995). All Gartnerkofel samples studied have Mn/Sr ratios of < 5 (data of Klein 1991).

It is interesting that the general warming trend across the Tesero Member is compatible with the warming across the

**Table 1** Carbon, carbonate and organic carbon isotope, and sulfur and sulfur isotope data for the Gartnerkofel core

Sample	Depth (m)	This paper		Klein (1991)	Magaritz and Holser (1991)			Klein (1991)	Pak and Holser (1991)
		C <sub>org</sub> (ppm)	δ <sup>13</sup> C <sub>org</sub> (‰)	C <sub>org</sub> (ppm)	δ <sup>13</sup> C <sub>carb</sub> (‰)	δ <sup>18</sup> O (‰)	δ <sup>13</sup> C <sub>org</sub> –δ <sup>13</sup> C <sub>carb</sub>	S (ppm)	δ <sup>34</sup> S (‰)
46	115.95	152		1150	1.25	– 4.76		72	
58	130.55	9		650	1.14	– 5.47		19	
67	143.26	197	– 26.67	840	1.58	– 3.62	– 28.25	200	
79	158.33	16		550	1.35	– 3.83		65	
89	171.33	689	– 27.88	650	1.12	– 4.20	– 29.00	158	
98	180.33	435	– 25.46	2700	0.31	– 4.89	– 25.77	75	
		376	– 25.90				– 25.90		
110	184.43	82	– 26.21	730	– 0.79	– 4.59	– 25.42	162	
116	185.51	145	– 26.19	1080	– 0.97	– 4.31	– 25.22	201	– 19.5
120	186.15	65	– 25.82	680	– 0.83	– 4.19	– 24.99	550	
125	186.93	392	– 28.22		– 0.44	– 4.69	– 27.78	200	
		391	– 27.83	990			– 27.83		
135	189.23	472	– 28.85	1150	0.48	– 4.44	– 29.33	230	
		450	– 28.41				– 28.41		
148	193.00	485	– 28.09	1350	– 0.67	– 2.25	– 27.42	242	
		495	– 28.13				– 28.13		
	<b>202.00</b>	<b>900</b>	<b>– 26.00</b>	<b>900</b>	<b>0.58</b>		<b>– 26.58</b>		
171	207.14	260	– 32.00	1650	0.26	– 7.21	– 32.26	31	
181	214.25			1040	– 1.14	– 3.82		222	
182	215.07	1960	– 32.10	1630	– 1.41	– 5.14	– 30.69	495	
		2044	– 31.82				– 31.82		
183	215.35			1920	– 1.28	– 3.68		6680	– 23.3
184	215.70			1070	– 0.93	– 7.44		2285	
185	216.30			2530				3540	
186	216.62	4624	– 28.67	1180	– 1.12	– 4.96	– 27.55	670	
187	219.70	700	– 30.66	1490	– 1.15	– 4.44	– 29.51	5120	
		724	– 31.01				– 31.01		
188	220.10	<b>1700</b>	– 29.90	1660	– 1.39	– 4.55	– 28.51	5655	
189	220.20			1650	– 1.57	– 4.46		6890	
190	220.35			5500	– 1.50	– 6.51		16,700	– 26.8
191	221.01	411	– 27.68	970	– 1.28	– 3.99	– 26.40	5440	– 25.3
		402	– 28.38				– 28.38		– 25.0
192	222.08			3950	– 1.14	– 5.12		1230	– 27.1
193	222.20			3540	– 1.01	– 4.98		33,100	– 28.8
194	222.35			1490	– 0.75	– 4.26		182	
194c	223.02	611	– 27.88		– 0.57	– 4.44	– 27.31		
Sample	Depth (m)	This paper		Klein (1991)	Magaritz and Holser (1991)			Klein (1991)	
		C <sub>org</sub> (ppm)	δ <sup>13</sup> C <sub>org</sub> (‰)	C <sub>org</sub> (ppm)	δ <sup>13</sup> C <sub>carb</sub> (‰)	δ <sup>18</sup> O (‰)	δ <sup>13</sup> C <sub>org</sub> –δ <sup>13</sup> C <sub>carb</sub>	S (ppm)	
195	223.94	152	– 26.20	650	– 0.88	– 4.10	– 25.32	191.00	
	<b>224.00</b>	<b>700</b>	<b>– 27.10</b>		<b>– 0.88</b>		<b>– 26.22</b>		
196b	225.01	410	– 26.41		0.33	– 4.38	– 26.74		
198	226.00	163	– 26.00	650	0.81	– 4.25	– 26.81	16.00	
198c	227.02	299			1.08	– 4.52			
199b	228.04	202	– 26.76		1.33	– 4.49	– 28.09		
			– 27.78				– 27.78		



**Table 1** continued

Sample	Depth (m)	This paper		Klein (1991)	Magaritz and Holser (1991)			Klein (1991)
		C <sub>org</sub> (ppm)	δ <sup>13</sup> C <sub>org</sub> (‰)	C <sub>org</sub> (ppm)	δ <sup>13</sup> C <sub>carb</sub> (‰)	δ <sup>18</sup> O (‰)	δ <sup>13</sup> C <sub>org</sub> –δ <sup>13</sup> C <sub>carb</sub>	S (ppm)
201	229.12	22		650		– 4.06		18.00
204	229.92	236		840	1.10	– 4.42		120.00
204c	230.60	332	– 26.74		1.43	– 4.63	– 28.17	
206	231.25	153		670	1.51	– 4.82		148.00
208	231.72	105	– 24.21	590	1.62	– 4.79	– 25.83	134.00
	<b>234.00</b>	<b>800</b>	– <b>25.20</b>		<b>1.74</b>		– 26.94	
	<b>235.00</b>	<b>600</b>	– <b>24.30</b>		<b>1.64</b>		– 25.94	
	<b>236.00</b>	<b>1500</b>	– <b>24.50</b>		<b>1.79</b>		– 26.29	
	<b>240.00</b>	<b>600</b>	– <b>24.10</b>		<b>1.92</b>		– 26.02	
	<b>241.00</b>	<b>600</b>	– <b>26.60</b>		<b>1.98</b>		– 28.58	
218	241.89	442	– 25.91	850	2.07	– 3.85	– 27.98	180.00
	<b>243.00</b>	<b>700</b>	– <b>24.10</b>		<b>1.86</b>		– <b>25.96</b>	
	<b>244.00</b>	<b>1000</b>	– <b>24.70</b>		<b>1.75</b>		– <b>26.45</b>	
223	251.00	592	– 35.01	3070	2.27	– 2.04	– 37.28	183.00
		590	– 34.70				– 34.70	
	<b>252.00</b>	<b>800</b>	– <b>39.00</b>		<b>2.69</b>		– 41.69	
	<b>254.00</b>	<b>1000</b>	– <b>24.50</b>		<b>2.12</b>		– 26.62	
	<b>267.00</b>	<b>700</b>	– <b>23.90</b>		<b>2.83</b>		– 26.73	
	<b>268.00</b>	<b>3400</b>	– <b>32.50</b>		<b>2.13</b>		– 34.63	
	<b>277.00</b>	<b>900</b>	– <b>23.80</b>		<b>2.03</b>		– 25.83	
247	277.98	26			2.52	0.35		140.00
255	286.33	176	– 38.26	1300	2.74	– 1.73	– 41.00	58.00
268	296.40	15		650	3.32	– 1.09		120.00
273	301.10	13		570	2.94	– 1.65		70.00
	<b>306.00</b>	<b>800</b>	– <b>24.50</b>		<b>2.95</b>		– <b>27.45</b>	
	<b>310.00</b>	<b>700</b>	– <b>25.30</b>		<b>3.02</b>		– <b>28.32</b>	
280	311.34	167		650	3.19	– 0.11		94.00
	<b>320.00</b>	<b>800</b>	– <b>23.10</b>		<b>2.66</b>		– <b>25.76</b>	
301	330.00	257	– 26.35		3.28	– 0.08	– 29.63	75.00

Bold—data from Magaritz et al. (1992)

Permian–Triassic boundary in China inferred from conodont apatite (Sun et al. 2012). The calculated seawater temperatures for Gartnerkofel based on Sun et al.'s (2012) methods, but using bulk δ<sup>18</sup>O<sub>carb</sub> values, show a low of – 10 °C in the Ostracod unit rising to + 6 to + 26 °C in the overlying units. The Ostracod unit temperatures are unreasonably low, but may be caused by variable salinities in this sabkha-type environment (Mette and Roobahani 2012). The higher temperatures are not inconsistent with a modern tropical carbonate environment like the Persian Gulf, where the lagoons and the open ocean can reach 24–32 °C and the coastal sabkhas can occasionally dip as low as 0 °C (Al-Farraj 2005; Warren 2006).

Sulfur concentrations from Klein (1991) are generally very low and less than 0.02%. Only one interval between 215 and 222 m contains higher values generally greater than 0.50% and range up to a maximum of 3.31% and these are associated with early diagenetic framboidal pyrite developed under anoxic conditions (Wilkin et al. 1996). The few available δ<sup>34</sup>S values of pyrite from Pak and Holser (1991) range from – 28.8‰ to – 19.5‰. An up section trend of increasing δ<sup>34</sup>S values matches a decreasing trend in sulfur concentrations (Fig. 3).

δ<sup>34</sup>S values of pyrite reflect the relative abundance of pyrite that formed within the water-column (syngenetic) and within the sediments (diagenetic), with lower values

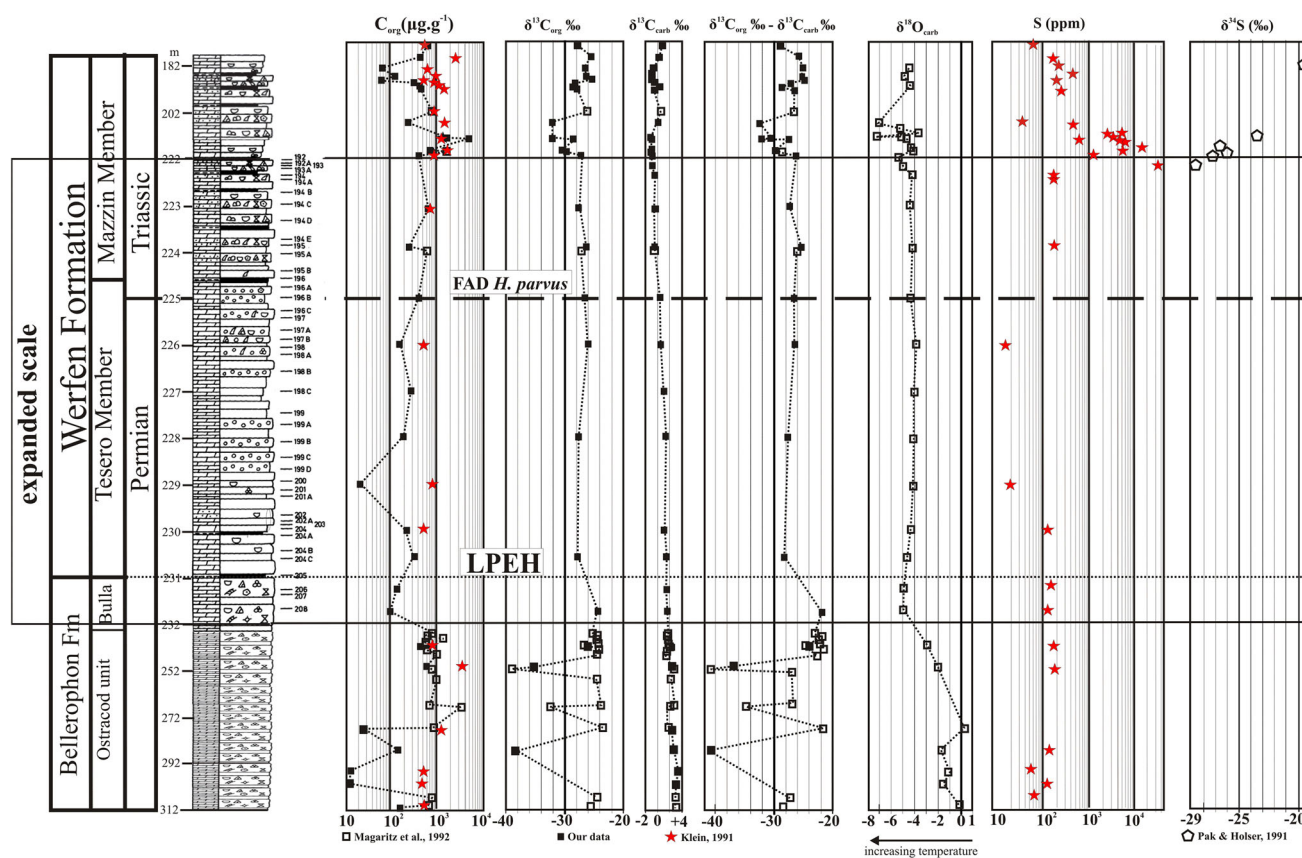


**Fig. 3** Late Permian to Early Triassic section of Gartnerkofel core (Holser et al. 1991; Schönlaub 1991); organic carbon and organic carbon isotope plots (this study); organic carbon plots from data in Klein 1991); carbonate and oxygen isotope plots from data in Magaritz and Holser (1991); S and S isotope plots from data in Klein (1991), Pak and Holser (1991) (see Table 1). Note expanded scale from 232 to 222 m depth

generally reflecting an increase in syngenetic pyrite due to anoxic or euxinic waters. The Tesero Member of the Bulla PTR section contains two relative minima in  $\delta^{34}\text{S}$  values of sulfide around  $-30\text{‰}$  with increases in S concentrations and S/C<sub>org</sub> ratios (Gorjan et al. 2007). The values in these intervals reflect an anoxic or euxinic water-column in the Tesero Member (Gorjan et al. 2007), and similar values are recorded at multiple locations after the LPEH (Shen et al. 2016 and references therein). At Gartnerkofel, the sharp increase in S concentrations and low values of  $\delta^{34}\text{S}$  in the Mazzin Member suggests an additional anoxic or euxinic interval in the Early Triassic, extending the record of transient anoxic intervals from the Tesero Member of the Bulla section.

## 5 Discussion and comparisons

Carbon isotope fluctuations in marine carbonates and marine plankton reflect the dissolved inorganic carbon reservoir in seawater. Organic carbon isotope fluctuations reflect the proportions contributed by marine and continental organic matter as well as by the contribution of

green sulfur bacteria growing in anoxic conditions—negative trends in organic carbon isotope values have been used to infer anoxia (Berner 2005).

The strong fluctuations in  $\delta^{13}\text{C}_{\text{org}}$  values across the Permian–Triassic boundary in Alpine sections are readily attributable to variations in the proportions of marine versus terrestrial organic matter (Kraus et al. 2013). The range of values of  $\delta^{13}\text{C}_{\text{org}}$  reported for modern terrestrial higher plants (average  $-26.1\text{‰}$ ), differs greatly from those for modern marine phytoplankton (average  $-17.7\text{‰}$ ) (Wickman 1952; Craig 1953; Smith and Epstein 1971). Changes in  $\delta^{13}\text{C}_{\text{org}}$  values of up to  $6.0\text{‰}$ , (from  $\sim -19\text{‰}$  to  $-25\text{‰}$ ) were measured across the Pleistocene–Holocene boundary in cores from the Gulf of Mexico abyssal plain, reflecting increased transport of terrestrial plant remains from re-established Holocene lowland forests to the Gulf basin (Newman et al. 1973). In the Quaternary, therefore, increased land plant input is marked by more negative  $\delta^{13}\text{C}_{\text{org}}$  values.

In contrast to modern organics, Permian plant material has heavier carbon isotope values ( $\delta^{13}\text{C} = -24\text{‰}$ ) compared with Permian plankton such as acritarchs ( $\delta^{13}\text{C} = -30\text{‰}$ ) (Faure et al. 1990; Strauss and Peters-

Kottig 2003; Herrmann et al. 2012). The difference from modern situations is because plants with C4 metabolism (all angiosperms) which have higher  $\delta^{13}\text{C}_{\text{org}}$  values between  $-8\%$  and  $-15\%$ , did not evolve until the Cretaceous (O'Leary 1988). Kraus et al. (2013) noted that the Alpine PTR sections from near shore to offshore showed the same organic carbon isotope trends but that the more offshore sections showed lighter, more negative values, consistent with greater plankton and lesser land plant input. Furthermore, their zigzag fluctuations in  $\delta^{13}\text{C}_{\text{org}}$  of up to  $4\%$  in the Tesero Member are most plausibly caused by variations in land versus marine organic content, especially as the  $\delta^{13}\text{C}_{\text{carb}}$  values do not change much. In contrast to Kraus et al.'s (2013) results, however, our main zigzag fluctuations occur lower down in the Bulla Formation, while their fluctuations in the Tesero member (admittedly based on much closer spaced samples) are not seen in our Tesero Member samples (Table 1, Fig. 3).

The two very negative  $\delta^{13}\text{C}_{\text{org}}$  peaks at 251/2 ( $-35\%$ ,  $-39\%$ ) and 286 m ( $-38\%$ ) depth at Gartnerkofel suggest marine incursions into the variable salinity Bellerophon sabkha environment. These extreme negative  $\delta^{13}\text{C}_{\text{org}}$  values are, however, beyond the range of both mantle-derived ( $\delta^{13}\text{C} = -5\%$ ) and organic carbon, including sulphur bacteria ( $\delta^{13}\text{C} < -30\%$ ) sources and require methane input ( $\delta^{13}\text{C} = -60\%$ ) (Summons et al. 1994; Higgins and Schrag 2006; Retallack and Krull 2006; Taipale et al. 2015). Even the overlying Bulla and Werfen values need either almost pure marine organic sources or methane input—but the methane would need to be metabolized by organisms. One possibility is that the recently discovered 'methane-eating' *Methylobakter* is responsible (Ettwig et al. 2010). Since these use nitrate reduction in their metabolism, then they might be detected from nitrogen isotope studies (to be done).

Smaller  $\delta^{13}\text{C}_{\text{org}}$  fluctuations also occur above 222 m depth where pyrite, sulfur and, shortly above, carbon content increase, with a marked shift to lighter, more negative marine  $\delta^{13}\text{C}_{\text{org}}$  values (Holser et al. 1989), consistent with the continuing Early Triassic marine transgression. The subsequent shift to heavier less negative values above 207 m suggests input of land plant material during the earliest Triassic which is recorded in other Alpine sections (Sephton et al. 2002; Gorjan et al. 2008).

The Val Badia section shows great  $\delta^{13}\text{C}_{\text{org}}$  fluctuations during Late Permian Tesero Member times with a more detailed sampling than Gartnerkofel (Fig. 4). In fact, all the PTR boundary section along both the southern and northern sides of the Neotethys and on the South China microcontinent show marked positive shifts in  $\delta^{13}\text{C}_{\text{org}}$  values though not necessarily at the same time if the correlations are accurate (Figs. 4, 5). If caused by greater land plant input, however, and if they are synchronous, then the positive

shift is consistent with the destruction of land ecosystems and vegetation burning at this time, and with the marked negative shift in  $\delta^{13}\text{C}_{\text{carb}}$  at this time (Grasby et al. 2011; Retallack 2013).

In Kashmir In the transitional beds equivalent to the lower Tesero Member, zigzags in  $\delta^{13}\text{C}_{\text{org}}$  values (from  $-27\%$  to  $-23\%$ ) (Algeo et al. 2007) are due to values from the background clays (more negative) and bioclastic beds introduced from shallower water (less negative) (Fig. 4). In China, both Meishan and Shangsi show similar negative shifts in  $\delta^{13}\text{C}_{\text{carb}}$  but the  $\delta^{13}\text{C}_{\text{org}}$  shows somewhat divergent trends (Fig. 5). The Meishan section is, however, very condensed with several erosion surfaces which juxtapose very different isotope values: missing sediments needs to be taken into account (Zheng et al. 2013).

In all Tethyan sections noted here, the  $\delta^{13}\text{C}_{\text{org}} - \delta^{13}\text{C}_{\text{carb}}$  values are greater in the shallower water sections like Gartnerkofel and Val Badia than in the deeper shelf sections at Guryul ravine, Shangsi and Meishan (Figs. 4, 5), which is in keeping with the decreasing continental input noted in the Alps (Kraus et al. 2013).

If the zigzags in the organic carbon isotope curves between the LPEH and the base of the Triassic are due to different proportions of land- and marine-derived organic matter, then either a number of marine transgressions and regressions need to be considered (as they have in the past—e.g. Brandner et al. 2009) or climatically-or event-controlled variations need to be considered.

Though rapid eustatic changes of sea-level occur in glacial times, there is no evidence of a Latest Permian glaciation and, in fact, the evidence is for rapid and significant ocean warming at the time (Sun et al. 2012; Song et al. 2014), which would raise sea-level by many metres due to thermal expansion since a  $1\text{ }^{\circ}\text{C}$  rise in mean ocean temperature raises sea-level by 2 m (Southam and Hay 1981). Rising sea level during warming and bringing more marine conditions over the area during deposition of the Tesero Member would explain the gradually lighter trends in both  $\delta^{13}\text{C}_{\text{org}}$  and  $\delta^{13}\text{C}_{\text{carb}}$ . Climate warming is thus a possible control—but a marine transgression in the Latest Permian does not explain the spasmodic input of land-derived vegetation at the time, nor the extreme negative  $\delta^{13}\text{C}_{\text{org}}$  values.

Input by backwash of land-derived material during storms, or even tsunamis, may explain some of the positive  $\delta^{13}\text{C}_{\text{org}}$  shifts associated with land vegetation input, even as far as the apparently isolated Bahamian-type Tesero oolite platform. Tsunami deposits have been identified in the Latest Permian in Kashmir, India (Brookfield et al. 2013). Vast amounts of land-derived floating material were transported into and across the Pacific Ocean by the relatively small 2011 Japanese tsunami (Lebreton and Borrero



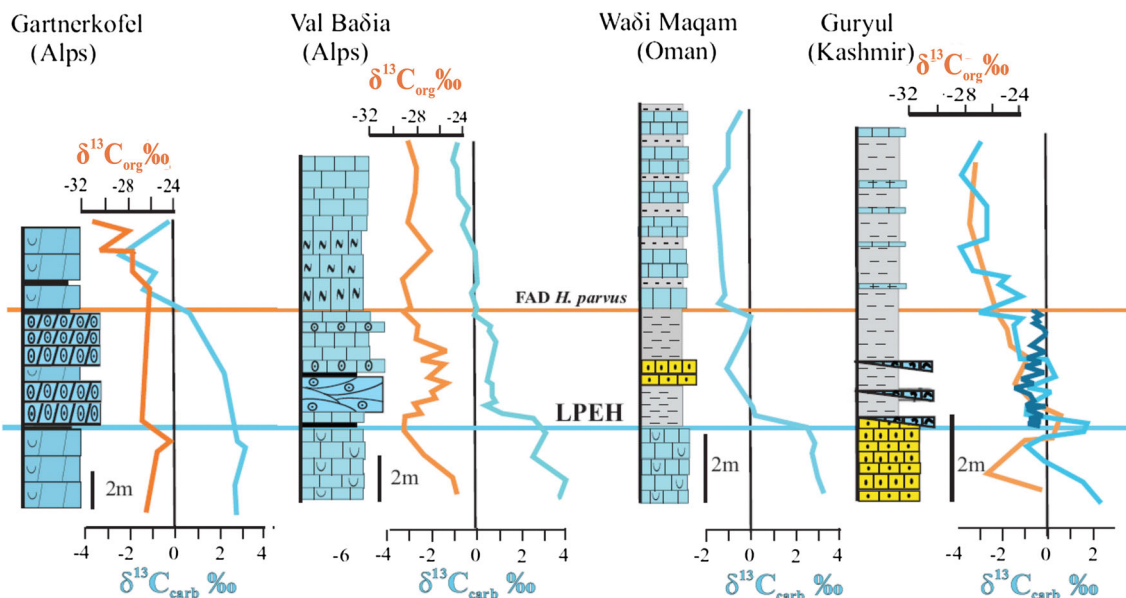


**Fig. 4** Comparison of Late Permian to Early Triassic organic carbon and carbonate C isotope plots for Gartnerkofel with various localities along southern Tethyan margin (modified from Korte et al. 2010) with additions and changes for Val Badia (Kraus et al. 2013), Guryul (Baud et al. 1996; Algeo et al. 2007). Height between LPEH and base of the Triassic has been standardized for all sections

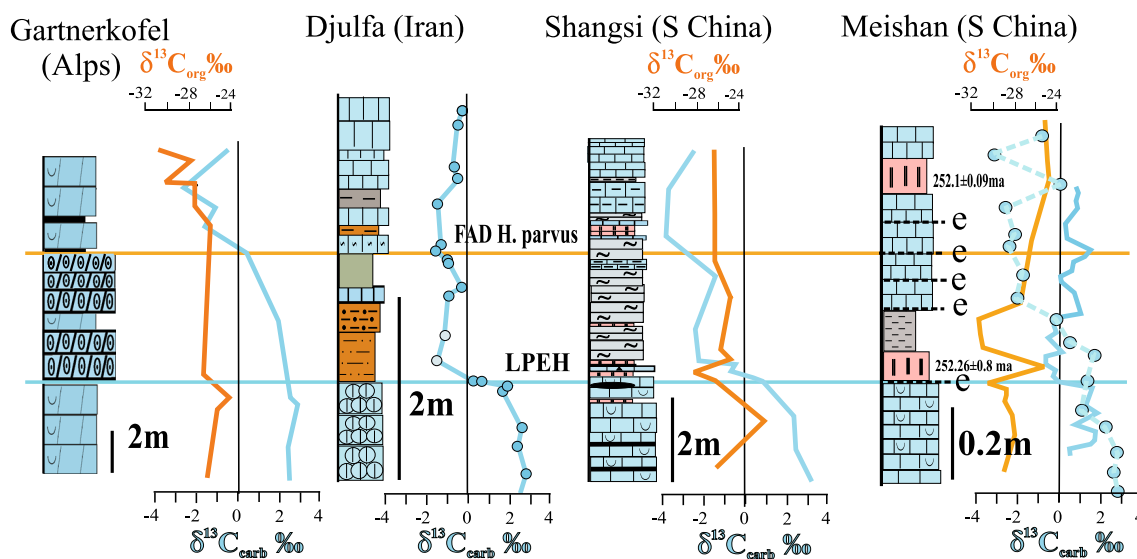


**Fig. 5** Comparison of Late Permian to Early Triassic organic carbon and carbonate C isotope plots for Gartnerkofel with various localities along northern Tethyan margin and South China (modified from Korte et al. 2010), with additions and changes for Djulfa (Kozur 2007; Ghaderi et al. 2014), Shangsi (Wignall et al. 1995; Jiang et al. 2011; Riccardi et al. 2007) Heping (Krull et al. 2004). Height between LPEH and base of the Triassic has been standardized for all sections

2013). The Tesero oolitic beds, with their hummocky cross-stratification and great extent (Brandner et al. 2009) are also possible tsunami rather than simple storm deposits.

## 6 Conclusions

A detailed carbon isotope curve across the Permian–Triassic boundary for the thoroughly studied Gartnerkofel core shows  $\delta^{13}\text{C}_{\text{org}}$  values generally become more negative upwards in parallel with the  $\delta^{13}\text{C}_{\text{carb}}$  values showing that atmospheric and oceanic carbon dioxide controlled both. Several extreme  $\delta^{13}\text{C}_{\text{org}}$  excursions, expressed in the

$\delta^{13}\text{C}_{\text{org}}-\delta^{13}\text{C}_{\text{carb}}$  values are attributed to periodic input of land vegetation either by storms or tsunamis. The overall trend of both  $\delta^{13}\text{C}_{\text{org}}$  and  $\delta^{13}\text{C}_{\text{carb}}$  values follow the other studied sections in the Alps and both northern and southern edges of the NeoTethys Ocean.

**Acknowledgements** We thank R. Schmitt for donating the samples and J. Gibson for making the C isotope measurements. We appreciate the comments of Elke Schneebeli-Hermann on an earlier draft of the manuscript.

#### Compliance with ethical standards

**Conflict of interest** All authors declare that they have no conflict of interest.

## References

- Al-Farraj A (2005) An evolutionary model for sabkha development on the north coast of the UAE. *J Arid Environ* 63:740–755
- Algeo TJ, Hannigan R, Rowe H, Brookfield ME, Baud A, Krystyn L, Ellwood B (2007) Sequencing events across the Permian–Triassic boundary, Guryul Ravine (Kashmir, India). *Palaeogeogr Palaeoclimatol Palaeoecol* 252:328–346
- Baud A, Atudorei V, Sharp Z (1996) Late Permian and Early Triassic evolution of the northern Indian margin: carbon isotope and sequence stratigraphy. *Geodinamica Acta (Paris)* 9:57–77
- Berner RA (2005) The carbon and sulfur cycles and atmospheric oxygen from Middle Permian to Middle Triassic. *Am J Sci* 69:3211–3217
- Boeckelmann K, Magaritz M (1991) The Permian–Triassic of the Gartnerkofel-1 core (Carnic Alps, Austria): dolomitization of the Permian–Triassic sequence. *Abh Geologischen Bundesanstalt* 45:61–68
- Brand U, Veizer J (1980) Chemical diagenesis of a multicomponent carbonate system, 1. Trace elements. *J Sediment Petrol* 50:1219–1236
- Brandner R (1988) The Permian–Triassic boundary in the Dolomites (Southern Alps, Italy), San Antonio section. *Ber Geologischen Bundesanstalt* 15:49–56
- Brandner R, Horacek M, Keim L, Scholger R (2009) The Pufels/Bulla road section: deciphering environmental changes across the Permian–Triassic boundary to Olenekian by integrated litho-, magneto- and isotope stratigraphy. A field guide. *Geol Alp* 6:116–132
- Brandner R, Horacek M, Keim L (2012) Permian–Triassic-boundary and lower Triassic in the Dolomites, Southern Alps (Italy). *J Alp Geol* 55:375–400
- Brookfield ME, Algeo TJ, Hannigan R, Williams J, Bhat GM (2013) Shaken and stirred: seismites and Tsunamites at the Permian–Triassic boundary, Guryul Ravine, Kashmir, India. *Palaios* 28:568–582
- Buggisch W, Noé S (1986) Upper Permian and Permian–Triassic boundary of the Carnian (Bellerophon Formation, Tesero horizon, northern Italy). *Mem Soc Géol d'Italia* 34:91–106
- Craig H (1953) The geochemistry of the stable carbon isotopes. *Geochim Cosmochim Acta* 3:53–92
- Dogliani C (1987) Tectonics of the Dolomites (Southern Alps, northern Italy). *J Struct Geol* 9:181–193
- Ettwig KF, Butler MK, Le Paslier D, Pelletier E, Mangenot S, Kuypers MMM, Schreiber F, Dutilh BE, Zedelius J, De Beer D, Gloerich J, Wessels HJCT, Van Alen T, Luesken F, Wu ML, Van De Pas-Schoonen KT, Op Den Camp HJM, Janssen-Megens EM, Francoijs KJ, Stunnenberg H, Weissenbach J, Jetten MSM, Strous M (2010) Nitrite-driven anaerobic methane oxidation by oxygenic bacteria. *Nature* 464:543–548
- Farabegoli E, Tonidandel D (2012) Stratigrafia e facies al limite Permiano-Triassico nell dolomite occidentali (Provincia di Bolzano, Italia): una revisione. *Geol Alp* 9:120–155
- Farabegoli E, Perri MC, Posenato R (2007) Environmental and biotic changes across the Permian–Triassic boundary in western Tethys: the Bulla parastratotype, Italy. *Glob Planet Change* 55:109–135
- Faure G, Mensing TM, Taylor EL (1990) Carbon isotope composition of Permian and Triassic plants in silicified peat, Transantarctic Mountains. *Antarct J Rev* 1990:26–27
- Gaetani M (2010) From Permian to Cretaceous: Africa as pivotal between extensions and rotations of Tethys and Atlantic Oceans. *J Virtual Explor.* <https://doi.org/10.3809/jvirtex.2010.00235>
- Ghaderi A, Leda L, Schobben M, Korn D, Ashouri AR (2014) High-resolution stratigraphy of the Changhsingian (Late Permian) successions of NW Iran and the Transcaucasus based on lithological features, conodonts and ammonoids. *Foss Rec* 17:41–57
- Gorjan P, Kaiho K, Kakegawa T, Niitsuma S, Chen ZQ, Kajiwaru Y, Nicora A (2007) Paleoredox, biotic and sulfur-isotopic changes associated with the end-Permian mass extinction in the western Tethys. *Chem Geol* 244:483–492
- Gorjan P, Kaiho K, Chen ZQ (2008) A carbon-isotope study of an end Permian mass-extinction horizon, Bulla, northern Italy: a negative  $\delta^{13}\text{C}$  shift prior to the marine extinction. *Terra Nova* 20:253–258
- Grasby SE, Sanei H, Beauchamp B (2011) Catastrophic dispersion of coal fly ash into oceans during the Latest Permian extinction. *Nat Geosci* 4:104–107
- Harris PM, Purkis SJ, Ellis J, Swart PK, Reijmer JGG (2015) Mapping bathymetry and depositional facies on Great Bahama Bank. *Sedimentology* 62:566–589
- Herrmann E, Hochuli PA, Bucher H, Roohi G (2012) Uppermost Permian to Middle Triassic palynology of the Salt Range and Surghar Range, Pakistan. *Rev Palaeobot Palynol* 169:61–965
- Higgins JA, Schrag DP (2006) Beyond methane: towards a theory for the Paleocene–Eocene thermal maximum. *Earth Planet Sci Lett* 245:523–537
- Holser WT, Schönlaub H-P, Attrep M Jr, Boeckelmann K, Klein P, Magaritz M, Orth CJ, Fenninger A, Jenny C, Kralik M, Mauritsch H, Pak E, Schramm J-M, Statteger K, Schmöller R (1989) A unique geochemical record at the Permian/Triassic boundary. *Nature* 337:39–44
- Holser WT, Schönlaub H-P, Boeckelmann K, Magaritz M (1991) The Permian–Triassic of the Gartnerkofel-1 core (Carnic Alps, Austria): synthesis and conclusions. *Abh Geologischen Bundesanstalt* 45:213–232
- Jiang H, Lai X, Yan C, Aldridge RJ, Wignall P, Sun Y (2011) Revised conodont zonation and conodont evolution across the Permian–Triassic boundary at the Shangsi section, Guangyuan, Sichuan, South China. *Glob Planet Change* 77:103–115
- Kaufman AJ, Knoll AH (1995) Neoproterozoic variations in the C-isotopic composition of seawater: stratigraphic and biogeochemical implications. *Precamb Res* 73:27–49
- Klein P (1991) The Permian–Triassic of the Gartnerkofel-1 core (Carnic Alps, Austria): geochemistry of common and trace elements 1—ICP, AAS and LECO. *Abh Geologischen Bundesanstalt* 45:109–121
- Korte Ch, Veizer J, Leythaeuser D, Below R, Schwartz L (2001) Evolution of Permian and lower Triassic  $\delta^{13}\text{C}$  in marine and terrigenous organic material. *Terra Nostra* 4:30–34

- Korte C, Pande P, Kalia P, Kozur HW, Joachimski MM, Oberhänsli H (2010) Massive volcanism at the Permian–Triassic boundary and its impact on the isotope composition of the ocean and atmosphere. *J Asian Earth Sci* 37:293–311
- Kozur HW (2007) Biostratigraphy and event stratigraphy in Iran around the Permian–Triassic Boundary (PTB): implications for the causes of the PTB biotic crisis. *Glob Planet Change* 55:155–176
- Kraus SH, Brandner R, Heubeck C, Kozur HW, Struck U, Korte C (2013) Carbon isotope signatures of Latest Permian marine successions of the Southern Alps suggest a continental runoff pulse enriched in land plant material. *Foss Rec* 16:97–109. <https://doi.org/10.1002/mmng201300004>
- Krull ES, Lehrmann DJ, Druke D, Kessel B, Yu YY, Li R (2004) Stable carbon isotope stratigraphy across the Permian–Triassic boundary in shallow marine carbonate platforms, Nanpanjiang basin, south China. *Palaeogeogr Palaeoclimatol Palaeoecol* 204:297–315. [https://doi.org/10.1016/S0031-0182\(03\)00732-6](https://doi.org/10.1016/S0031-0182(03)00732-6)
- Lebreton CCM, Borrero JC (2013) Modeling the transport and accumulation of floating debris generated by the 12 March, 2011 Tohoku tsunami. *Mar Pollut Bull* 66:53–58
- Magaritz M, Holser WT (1991) The Permian–Triassic of the Gartnerkofel-1 core (Carnic Alps, Austria): carbon and Oxygen isotope variations. *Abh Geologischen Bundesanstalt* 45:149–163
- Magaritz M, Krishnamurthy RV, Holser WT (1992) Parallel trends in organic and inorganic carbon isotopes across the Permian/Triassic boundary. *Am J Sci* 292:727–739
- Mette W, Roobahani P (2012) Late Permian (Changhsingian) ostracods of the Bellerophon Formation at Seis (Siusi) (Dolomites, Italy). *J Micropaleontol* 31:73–87
- Muttoni G, Dallanave E, Channell JET (2013) The drift history of Adria and Africa from 280 Ma to present, Jurassic true polar wandering, and zonal climate control on Tethyan sedimentary facies. *Palaeogeogr Palaeoclimatol Palaeoecol* 386:415–435
- Newman JW, Parker PL, Behrens EW (1973) Organic carbon isotope ratios in Quaternary cores from the Gulf of Mexico. *Geochim Cosmochim Acta* 37:225–238
- Noé SU (1987) Facies and palaeogeography of the marine Upper Permian and of the Permian–Triassic boundary in the southern Alps (Bellerophon Formation, Tesero horizon). *Facies* 16:89–142
- O’Leary MH (1988) Carbon isotopes in photosynthesis. *Bioscience* 38:328–336
- Pak EN, Holser WT (1991) The Permian–Triassic of the Gartnerkofel-1 core (Carnic Alps, Austria): sulfur isotopes. *Abh Geologischen Bundesanstalt* 45:165–167
- Posenato R (2009) Survival patterns of macrobenthic marine assemblages during the end-Permian mass extinction in the western Tethys (Dolomites, Italy). *Palaeogeogr Palaeoclimatol Palaeoecol* 280:150–167
- Retallack GJ (2013) Permian and Triassic greenhouse crises. *Gondwana Res* 24:90–103
- Retallack GJ, Krull ES (2006) Carbon isotopic fractionation in lipids from methanotrophic bacteria: relevance for interpretation of the geochemical record of biomarkers. *Geol Soc Am Spec Pap* 399:249–268
- Riccardi A, Kump LR, Arthur MA, D’Hondt S (2007) Carbon isotope evidence for chemocline upward excursions during the end-Permian event. *Palaeogeogr Palaeoclimatol Palaeoecol* 248:73–81
- Schönlaub H-P (1991) The Permian–Triassic of the Gartnerkofel-1 core (Carnic Alps, Austria): conodont biostratigraphy. *Abh Geologischen Bundesanstalt* 45:79–98
- Sephton MA, Looey CV, Veeffkind RJ, Brinkhuis H, De Leeuw JW, Visscher H (2002) Synchronous record of  $\delta^{13}\text{C}$  shift in the oceans and atmosphere at the end of the Permian. *Geol Soc Am Spec Pap* 356:455–462
- Shen J, Feng Q, Algeo TJ, Li C, Planavsky NJ, Zhou L, Zhang M (2016) Two pulses of oceanic environmental disturbance during the Permian–Triassic boundary crisis. *Earth Planet Sci Lett* 443:139–152
- Smith BN, Epstein S (1971) Two categories of  $\delta^{13}\text{C}$  ratios for higher plants. *Plant Physiol* 47:380–384
- Song H, Wignall PB, Daoliang C, Tong J, Sun Y, Song H, He W, Tian L (2014) Anoxia/high temperature double whammy during the Permian–Triassic marine crisis and its aftermath. *Sci Rep*. <https://doi.org/10.1038/srep04132>
- Southam JR, Hay WW (1981) Global sedimentary mass balance and sea level changes. In: Emiliani C (ed) *The sea*, vol 7. Wiley, New York, pp 1617–1684
- Strauss H, Peters-Kottig W (2003) The Paleozoic to Mesozoic carbon cycle revisited: the carbon isotopic composition of terrestrial organic matter. *Geochem Geophys Geosyst* 4:1–15. <https://doi.org/10.1029/2003GC000555>
- Summons RE, Jahnke LL, Roksandic Z (1994) Carbon isotopic fractionation in lipids from methanotrophic bacteria: relevance for interpretation of the geochemical record of biomarkers. *Geochim Cosmochim Acta* 58:2853–2863
- Sun Y, Joachimski MM, Wignall PB, Yan Chumbo, Chen Yanlong, Jiang Haishul, Lai Xulong (2012) Lethally hot temperatures during the early Triassic greenhouse. *Science* 338:366–370
- Taipale SJ, Peltomaa E, Hiltunen M, Jones RI, Hahn MW, Biasi C, Brett MT (2015) Inferring phytoplankton, terrestrial plant and bacteria bulk  $\delta^{13}\text{C}$  values from compound specific analyses of lipids and fatty acids. *PLoS ONE* 10(7):e0133974. <https://doi.org/10.1371/journal.pone.0133974>
- Warren JK (2006) *Evaporites: sediments, resources and hydrocarbons*. Springer, Berlin
- Wickman FE (1952) Variations in the relative abundance of the carbon isotopes in plants. *Geochim Cosmochim Acta* 2:243–252
- Wignall PB, Hallam A, Xulong Lai, Fengqing Yang (1995) Palaeoenvironmental changes across the Permian/Triassic at Shangsi (N. Sichuan, China). *Hist Biol* 10:175–189
- Wilkin RT, Barnes HJ, Brantley SL (1996) The size distribution of framboidal pyrite in modern sediments: an indicator of redox conditions. *Geochim Cosmochim Acta* 60:3897–3912
- Wolbach WS, Anders E (1989) Elemental carbon in sediments: determination and isotopic analysis in the presence of Kerogen. *Geochim Cosmochim Acta* 53:1637–1647. [https://doi.org/10.1016/0016-7037\(89\)90245-7](https://doi.org/10.1016/0016-7037(89)90245-7)
- Wolbach WS, Roegge DR, Gilmour I (1994) The Permian–Triassic of the Gartnerkofel-1 core (Carnic Alps, Austria): organic carbon isotope variation. In: Conference on new developments regarding the K/T event and other catastrophes in earth history. Lunar and Planetary Institute, Houston, pp 133–134
- Zheng QF, Cao CQ, Zhang MY (2013) Sedimentary features of the Permian–Triassic boundary sequence of the Meishan section in Changxing County, Zhejiang Province. *Sci China Earth Sci* 56:56–969